Received: 27 December 2019 | Revised: 6 March 2020 | Accepted: 23 March 2020

DOI: 10.1111/ffe.13232

ORIGINAL CONTRIBUTION

FFEMS Fatigue & Fracture of Engineering Materials & Structures WILEY

Requirements for stress gradient-based fatigue assessment of notched structures according to theory of critical distance

Moritz Braun | **André Mischa Müller** | **Aleksandar-Saša Milaković** | **Wolfgang Fricke** | **Sören Ehlers**

Institute for Ship Structural Design and Analysis, Hamburg University of Technology, Hamburg, Germany

Correspondence
Moritz Braun, Hamburg University of Technology, Institute of Ship Structural Design and Analysis (M-10), Am Schwarzenberg Campus 4(C), D-21073 Hamburg, Germany.
Email: moritz.br@tuhh.de

Funding information
German Research Association of the Working Group of the Iron- and Metal-processing Industry e.V., Grant/Award Number: A301

Abstract

Notches, local stress raisers within structural components, are one of the most important locations for fatigue crack initiation. It is well known that fatigue is governed by the effective stresses in the vicinity of notches. Within this study, differences in prediction accuracy between different types of theory of critical distance methods, that is, point and line methods, are systematically investigated in conjunction with a sensitivity study regarding mesh refinement, assumed strength hypothesis and material behaviour. For this purpose, a finite element analysis parameter study on notched structures is performed and recommendations for the application of stress gradient methods are presented. Difference in effective stress of up to 30%, and hence a significant difference in fatigue life (e.g., 185% for a slope of S-N curve of $k = 4$), is found for typical notch shapes, for example, in welded joints.

KEYWORDS

critical distance, fatigue at notches, finite element analysis, notch fatigue analysis, notch sensitivity, stress gradient

1 | INTRODUCTION

Notches, a form of geometric discontinuity within structural components, are one of the most significant locations for fatigue crack initiation due to local stress and strain concentrations. Thus, fatigue damage often originates at notches. The reliable assessment of fatigue strength is thus very important for the purpose of cost reduction and risk assessment.

As notches lead to high local stresses and a multiaxial stress/strain state, they represent an area which is of great interest for fatigue limit state design of structures; this is especially true because their fatigue life is significantly reduced compared with unnotched structures. In fatigue assessment of notched structures, it is well known that the fatigue strength is not governed by the linear elastic maximum stress at the notch tip, but rather by the stress field surrounding the notch.[1] The main reasons are the high stress field gradients at sharp notches, the local plastic zone and initial damage in the form of microscopic cracks.[2] Moreover, assessment based on the elastic peak stresses fails to predict size effects.[3]

Since the beginning of fatigue strength assessment, many different approaches to determine effective stress parameters for the stress fields surrounding notches have been developed. Later, these approaches have been

extended and applied to welded joints.[4] All of them are based on the idea of taking into account the support effect of the material surrounding a local stress raiser by mapping the elastic stress field by a suitable functional[5] (cf. Berto et al.[6] or textbooks[7] regarding analytical functionals for the stress field).

A way of distinguishing different effective stress approaches is by considering dimensional space (e.g., point, line, area or volume). Because of increased computational power, such methods are more easily applicable nowadays. The point (PM) and line (LM) methods—based on the gradient of the stress acting perpendicular to the expected crack path—have gained especial interest, judging by the variety of investigated applications.[8–29]

The main advantage of gradient methods, compared with other fatigue assessment methods, is the possibility of taking thickness effects directly into account; see Hobbacher[30] regarding limitations to assess thickness effects with different fatigue assessment methods. Moreover, recent research results have shown that such methods can be applied to notches with significantly different proportions or strength grades, such as welded and post-weld treated joints at the same time[11,13]; in many technical fields, however, application of such methods is currently not possible because of guidelines and design codes that are limited to nominal, hot-spot, notch stress and fracture mechanics approaches.[31–33] Typically, as with every emerging method, general applicability has first to be proven by case studies. Moreover, increased prediction accuracy has to outweigh higher preparation efforts.

Of all effective stress methods, two versions of stress gradient methods have been popularly applied in the recent years. One of these approaches averages the stress over a certain microstructural support length ρ^* proposed by Neuber.[1] The underlying assumption is that crack initiation is controlled by the averaged stress in a small material volume (defined by the averaging length ρ^*) at the point of maximum stress.[34] A different idea, which was proposed shortly afterwards, defines the effective stress σ_{eff} as the value at a certain distance a from the root of a notch.[35] The idea behind this approach is that crack initiation is related to the effective stress evaluated at a material dependent critical depth a below the notch root surface.[34] Thus, the fatigue strength at notches is described by the fatigue notch factor K_{f}, which is related to the elastic notch stress concentration factor K_{t} with

$$K_{\mathrm{f}} = 1 + \frac{K_{\mathrm{t}} - 1}{1 + \frac{a}{r}}, \tag{1}$$

where r is the notch radius and K_{t} the ratio between the maximum stress at the notch root and the nominal stress. For design, however, it is more common to calculate fatigue life from effective stresses in conjunction with appropriate stress-life (S-N) curves than to calculate the fatigue notch factor K_{f}; see Radaj et al.[36]

Today, these methods are sometimes summarized under the term theory of critical distances (TCD).[2] In addition to PM, based on Peterson,[35] and LM, based on Neuber,[1,37] a number of other approaches take into account area or volume.[38–40] For typical notched structures like machinery components, stress gradient methods are regularly applied for fatigue assessment; however, gradient methods based on the TCD have successfully been applied to welded joints in recent years as well.[9,13,15] Interestingly, both PM and LM are assumed to result in equal stress values for certain distance of evaluation ratios.[41] A ratio of $a = \rho^*/4$ is expected to yield equal results, although differences in prediction accuracy between both have already been addressed.[3,17,20,34,42]

In high cycle fatigue assessment ($N > 10^4$), the lifetime N can by calculated by

$$N = N_{\mathrm{R}} \left(\frac{\Delta\sigma_{\mathrm{eff}}}{\Delta\sigma_{\mathrm{R}}} \right)^{-k}, \tag{2}$$

where $\Delta\sigma_{\mathrm{eff}}$ is the effective stress range and N_{R} is the reference number of cycles to failure with the corresponding reference fatigue strength $\Delta\sigma_{\mathrm{R}}$. By raising the stress to the power of the slope exponent k of a S-N or Wöhler curve, small differences in effective stress may lead to high deviation in estimated lifetime.

This study aims to contribute to the applicability of TCD for fatigue assessment by analysing the effect of notch geometry on fatigue strength, using stress gradient methods. In this context, the assumed ratio $a = \rho^*/4$ between PM and LM, expected to result in equal effective stresses, is analysed. For this investigation, finite element analysis is applied, starting with a parameter study regarding mesh requirements.

In literature, many cases report differences in prediction accuracy between different types of TCD methods.[3,9,17,20,42] To the author's knowledge, there has been no systematic investigation in conjunction with a sensitivity study for mesh refinement and assumed strength hypothesis. In order to reach a level of applicability in international standards and guidelines, meshing recommendations and clarity for differences in prediction accuracy are required. Hence, this study seeks to solve this problem by numerically analysing notched structures with varying geometry parameters, strength hypothesis and material behaviour (plane stress and plane strain).

2 | NOTCH PARAMETERS

Notches, as typical engineering stress raisers, can occur in many different shapes. For the scope of this paper, however, only u-type and v-type notches (with variable notch radius) are analysed in context of practical applications. In order to define the geometry of a notch, multiple parameters such as notch radius, notch depth and the opening angle[7] are required. Two of these parameters, the notch radius r and the opening angle ω, are shown in Figure 1A. The importance of notches in structural components is illustrated by engineering examples like welded joints (Figure 1B,C), additive manufactured parts (Figure 1D) and medical implants (Figure 1E).

3 | GRADIENT METHODS

As mentioned in Section 1, different forms of the TCD are currently used to determine the effective stress in order to evaluate the lifetime of a structural component (see Figure 2). One form of the TCD is the point method; this is based on the critical distance approach by Peterson[35] and defines effective stress as the stress value perpendicular to the root of the notch at a fixed distance. The effective stress σ_{eff} for the PM can thus be calculated by

$$\sigma_{\text{eff}} = \sigma_y\left(\theta = 0, s = \frac{L}{2}\right), \tag{3}$$

where σ_y is the stress at a certain distance perpendicular to the root of the notch (i.e., along the notch bisector) and θ and s are polar coordinates. Here, L is a material characteristic length dependent on the material, the number of cycles to failure[42] and the type of loading.[2,43] For the PM, it is assumed that failure occurs, if the effective stress range $\Delta\sigma_{\text{eff}}$ at $L/2$ is equal or exceeds the fatigue limit $\Delta\sigma_0$.[2] On the basis of fracture mechanics, it can be shown that the material characteristic length L is related to the fatigue crack propagation threshold ΔK_{th} and the fatigue limit with

$$L = \frac{1}{\pi}\left(\frac{\Delta K_{\text{th}}}{\Delta\sigma_0}\right)^2. \tag{4}$$

The material characteristic length L is thus directly related to the transition point between short and long crack growth.

A different form of the TCD to determine the effective stress is the LM. This approach, as opposed to the PM, averages the stress perpendicular to the root of notch over the material characteristic length to determine the effective stress.[1] The resulting effective stress can be calculated as follows[2]:

$$\sigma_{\text{eff}} = \frac{1}{2L}\int_0^{2L} \sigma_y(\theta = 0, s)\, ds. \tag{5}$$

The distance L to evaluate the stress henceforth refers to Neuber's[1] and Peterson's[35] initial propositions. In case of PM, the notation a ($a = L/2$), and for LM, ρ^* ($\rho^* = 2L$), will be used to distinguish both methods.

For some applications, values for different materials can be found in textbooks or publications[34,37]; however, for every new application material characteristic length, values have to be found by solving the inverse problem (i.e., finding the length parameter that describes a dataset best; see Santus et al.[17]). Typical values for welded joints

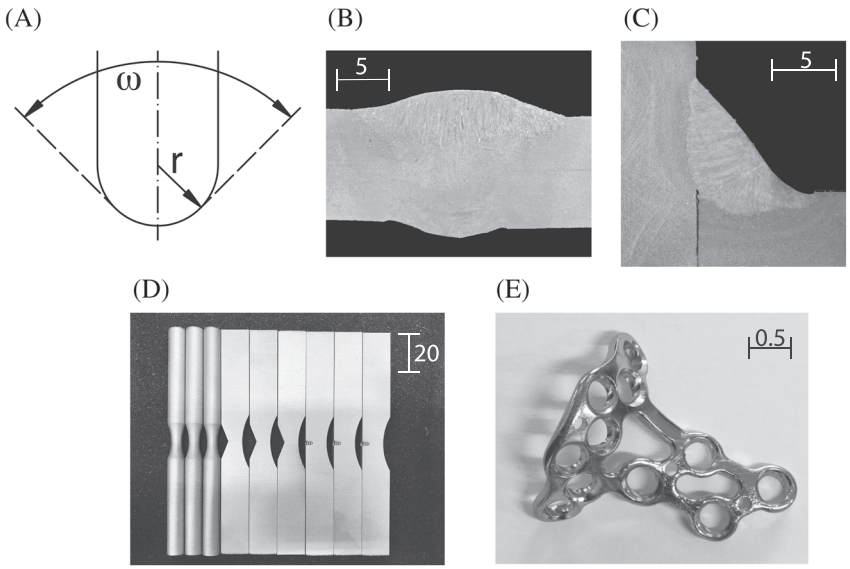

FIGURE 1 Schematic drawing of notch parameters (A), welded joints (B) and (C), additive manufactured parts (D) and medical implant (E); scale in millimetres

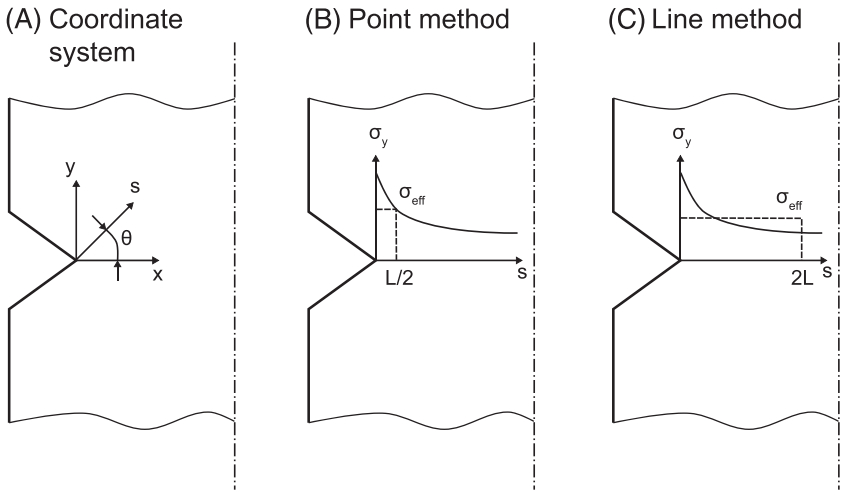

FIGURE 2 Stress gradient methods based on Louks and Susmel[20]

that are frequently found in literature are $\rho^* = 0.4$ mm and $a = 0.1$ mm.[9]

4 | DEFINITION OF NOTCHED GEOMETRY

The commercial software ANSYS is used to perform finite element analysis for the parameter study and the comparison of gradient methods. In this study, the two main parameters varied are the notch radius r and the opening angle ω. The depth of the notch is kept constant at 10 mm. Two opening angles ω are investigated (0° and 135°), both of which are frequently found in welded joints and notched structures. Notches at weld roots often approach opening angles close to 0° (i.e., almost crack like), whereas v-type notches with approximately 135° opening angles are typical for weld toes (see Figure 1). For the notch radius r, values of 0.05 and 0.5 mm (representing a sharp, almost crack-like and a blunt notch) are used within this study. Moreover, both values enable comparability with other studies.[7,44–46] An overview of the parameter combinations investigated are listed in Table 1.

The investigation of notch stress, in context of the aims described in Section 1, does not demand a particularly complex model. In order to investigate the aforementioned effects, a two-dimensional model is sufficient (see Baumgartner and Bruder[44] and Leitner et al.[47]); this also leads to a smaller computational effort. For the finite element analysis, typical material properties for steel are applied, which are summarized in Table 2.

A sketch of the half model is shown in Figure 3. The symmetry about the neutral axis is used to minimize computational effort. Parameters used as input data for the geometry of the model are marked in red, whereas blue indicates parameters that are dependent on one or more of the input parameters.

The radius of the notch r and the opening angle ω are the main parameters varied during the analysis (see Table 1). The depth of the notch d is set to 10 mm, as previously mentioned. Furthermore, the distance g between the root of the notch and the neutral axis is set to 10 mm, thus yielding a notch depth to height ratio of $d/h = 0.5$. The *load*, which is applied on the right end of the specimen, is specified as a unit stress (1 N mm^{-2}).

The number of elements n, which represent the circular arc of the notch, is defined as number of elements over 360° (full circle). Values for n are investigated as part of the parameter study. Although a finer mesh generally results in more accurate stress values, it is also more computationally expensive. As can be seen from Figure 3, the specimen is divided into two areas (one global area and one local area around the root of the notch) with the size of the area around the root of the notch defined by two parameters. One of them, the depth of the area r_1, is kept constant at 5 mm. The other, the angle φ, is a function of the opening angle ω ($\varphi = 180° - \omega$). Within this area, the element size e is

TABLE 1 Parameter combinations investigated

Notch radius r (mm)	Opening angle ω (°)
0.05	0°
0.05	135°
0.5	0°
0.5	135°

TABLE 2 Material properties

Young's modulus ($\frac{N}{mm^2}$)	Shear modulus ($\frac{N}{mm^2}$)	Poisson's ratio υ (−)
206000	$\frac{206000}{2\cdot(1+\upsilon)}$	0.3

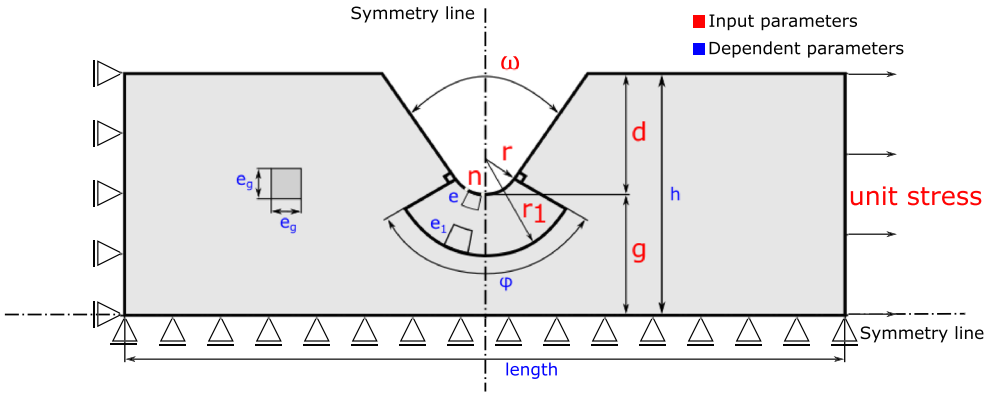

FIGURE 3 Specimen geometry [Colour figure can be viewed at wileyonlinelibrary.com]

dependent on two parameters: n (the number of elements over 360°) and the aspect ratio of the elements. In order to obtain accurate results with minimum preparation, the aspect ratio is set to one, although elements with an aspect ratio up to two (shorter in depth-direction) might reduce the number of elements required.[44] The global element size e_g is a function of the element size e_1 at the outer radius of the area around the root of the notch. This ensures the elements in the transition area remain well shaped, leading to a precise analysis.

The element type for the analysis is a 2D eight-node structural solid (plane183 in ANSYS) with plane strain condition. Figure 4 depicts an example of the performed simulation for $r = 0.05$ mm, $\omega = 0°$ and $n = 72$, with first principal nodal stress results.

First principal and von Mises nodal stress results are extracted along the notch bisector for each simulation. The evaluation of the stress gradient is subsequently performed using scripts in Matlab. Because polynomial curve fitting does not lead to a satisfying evaluation of the raw stress data, piecewise cubic hermite interpolating polynomial (PCHIP) curve fitting is applied. The PCHIP curve fitting is shape preserving, meaning that slopes at the evaluation points are chosen such that the interpolant preserves the shape of the data to be fitted. Numerical integration (trapezoidal rule) with $5{\cdot}10^{-4}$ mm increments is applied for averaging the stress gradient according to LM.

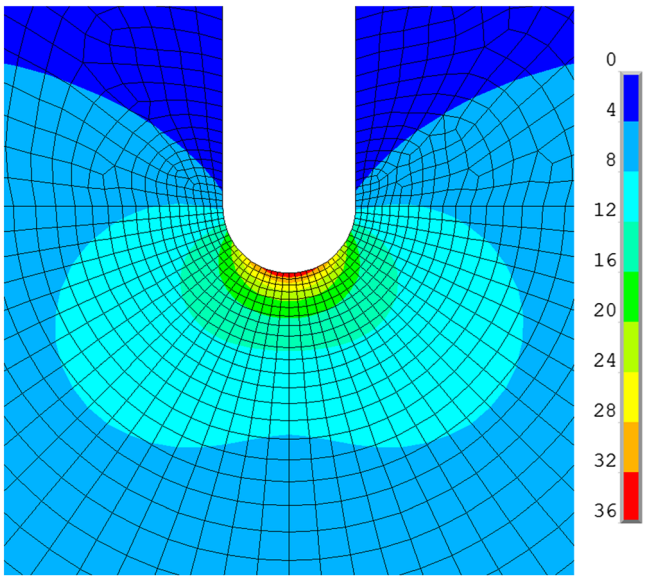

FIGURE 4 Meshed specimen and first principal nodal stress distribution for $r = 0.05$ mm, $\omega = 0°$ and $n = 72$ [Colour figure can be viewed at wileyonlinelibrary.com]

5 | MESHING REQUIREMENTS FOR STRESS GRADIENT METHODS

As mentioned in Section 1, the first part of the finite element analysis is a parameter study to determine the required number of elements n to calculate consistent stress results for application of stress gradient methods. This is achieved by determining values of n that yield an effective stress result with less than 1% deviation from the finest analysed mesh; these results will be presented later. On the basis of the assumption that fixed microstructural support length $\rho^* = 0.4$ mm for a cast iron-like microstructure of weld metal, Radaj[4] developed the effective notch stress concept widely applied for fatigue assessment of welded joints nowadays; because of its significance, this value will also be used as a reference in the present study.

The mesh generation, and thereby the required number of elements per 360°, is governed by the need for an element border at the notch bisector (see Figure 2). Given the definition of n, different elements are required to model the circular arc (i.e., $n/2$ for 0° and $n/8$ for 135°). Table 3 lists the range of values for n in combination with the parameters for the notch radius r and the opening angle ω of Table 1. Resulting meshes for $r = 0.05$ mm and $\omega = 0°$ are presented in Figure 5.

The results of the parameter study are shown in Figure 6 using the example of $r = 0.5$ mm and $\omega = 0°$.

TABLE 3 List of number of elements n over 360° for the investigated notch geometries

Elements over 360° n (−) for opening angle $\omega = 0°$	Elements over 360° n (−) for opening angle $\omega = 135°$
8	8
12	24
16	40
24	56
32	72
36	152
48	312
72	—
144	—
288	—

Each of the coloured lines in the five subfigures represent a different number of elements n over 360°. The three numbers in the notation of the simulations signify the following: mesh, element side ratio and number of elements over 360°.

Figure 6A presents the maximum principal stresses σ_1. In order to differentiate between the curves, a more detailed view of the stress is depicted over the first 0.5 mm in Figure 6B showing a clear difference between stress gradients for varying numbers of elements n. Notably, the curve for $n = 8$ deviates more than the other curves. Unsurprisingly, having a low number of elements inaccurately represents stress gradients. The effective stress σ_{eff} derived with LM is presented in Figure 6C. For comparison, the effective stress is normalized by the maximum effective stress for the first averaging length $\rho^* = 0.05$ mm with $\sigma_{\text{eff,norm}} = \sigma_{\text{eff}}/\sigma_{\text{eff,max}}$ in Figure 6D. On the basis of the graphs of Figure 6, the deviation between stress gradients for varying numbers of elements is hardly discernible. Even the most detailed plot, Figure 6B, indicates very similar trends for all curves. A more detailed presentation of the variation of normalized effective stress for averaging length $\rho^* = 0.4$ mm is given in Figure 7.

The number of elements n over 360° is on the horizontal axis and effective stress normalized by the maximum effective stress ($\sigma_{\text{eff,norm}} = \sigma_{\text{eff}}/\sigma_{\text{eff,max}}$) is on the vertical axis. The maximum effective stress is the value for the highest number of n, where convergence is expected based on the asymptotic behaviour of the graphs. The converged stress values are assumed to be found for $n = 288$ and $n = 312$, respectively. This definition of the normalized effective stress allows a direct comparison based on the percent deviation between the stress values and the converged stress. Within Figure 7, the trends of all four investigated parameter combinations (outlined in Table 1) are presented. Contrary to the impression of Figure 6, an error of up to approximately 6% is found. In order to reach an error less than 1% for effective stress values, the required number of quadratic elements n is 32 for $\omega = 0$. In contrast, the required number of elements for v-type notches with $\omega = 135°$ is only 24. These conclusions hold true for radii of both 0.05 and 0.5 mm.

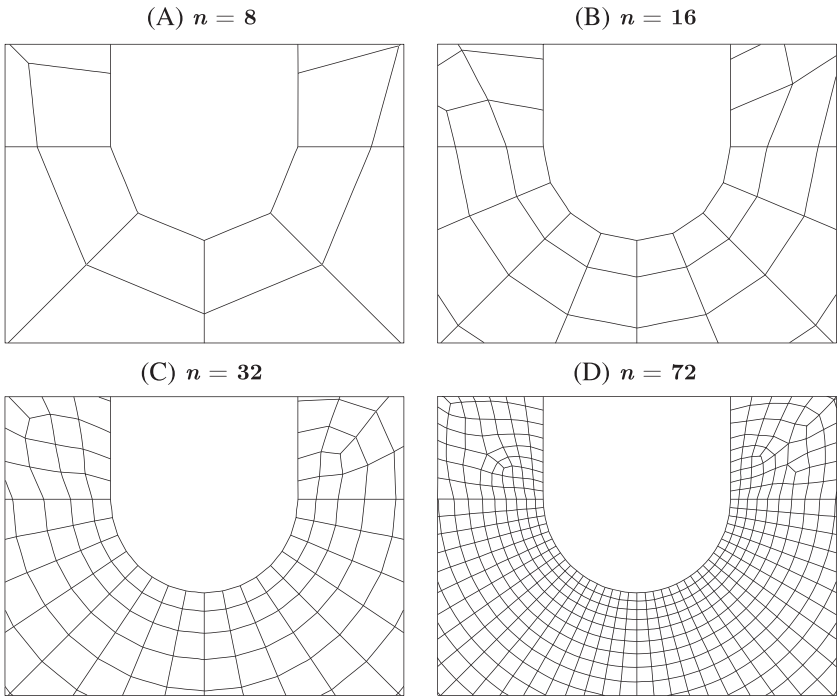

FIGURE 5 Resulting meshes for $r = 0.05$ mm, $\omega = 0°$ and $n = 8/16/32/72$

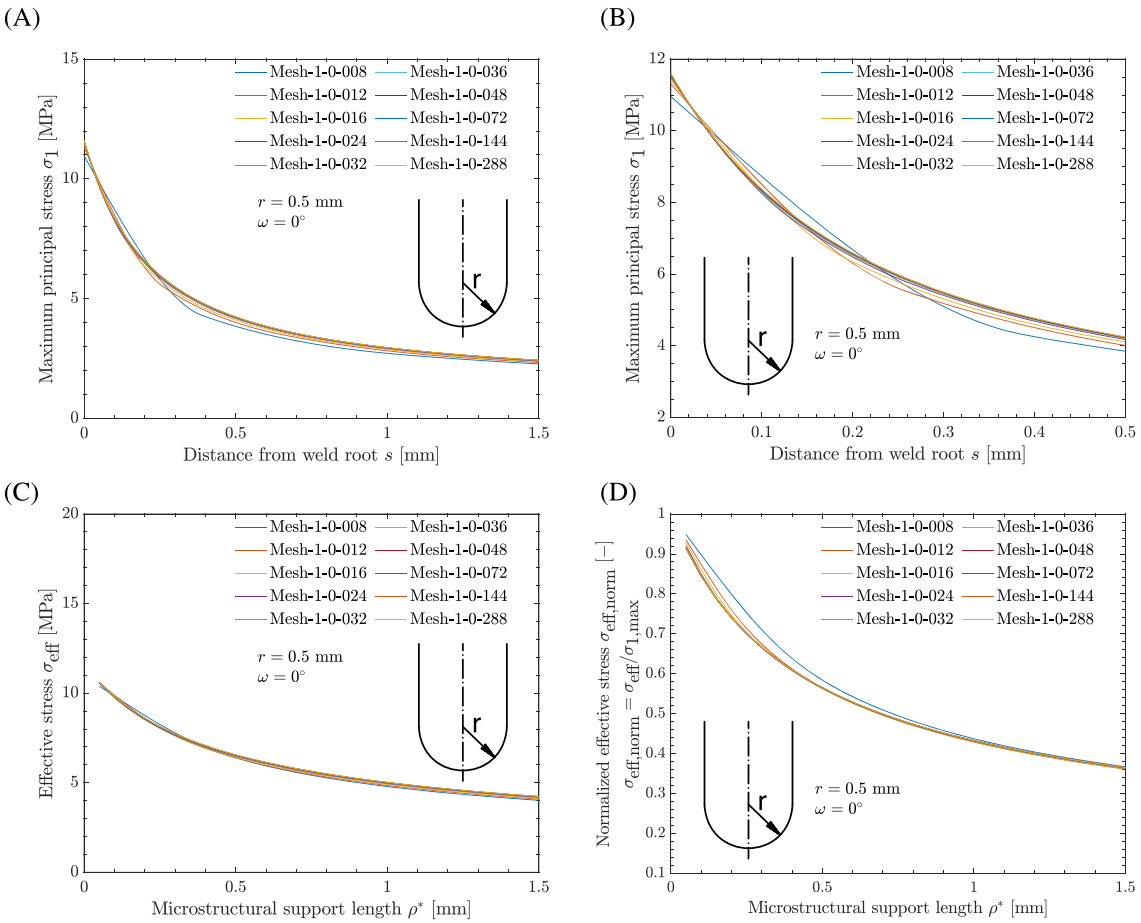

FIGURE 6 Principal stress in the range 0 to 1.5 mm (A) and 0 to 0.5 mm (B), effective stress (C) and normalized effective stress (D) distribution along bisector line for radius $r = 0.5$ mm and opening angle $\omega = 0°$, with an element aspect ratio of 1, for varying numbers of elements per 360° (from 8 to 288) [Colour figure can be viewed at wileyonlinelibrary.com]

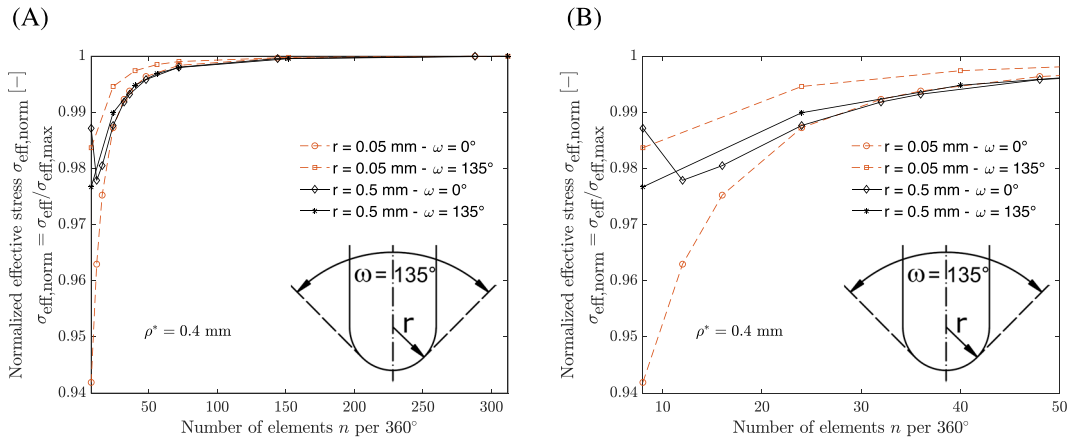

FIGURE 7 Convergence of effective stress results for (A) various numbers of elements n per 360° normalized by the effective stress at $\rho^* = 0.4$ mm and (B) detailed presentation for $n = 8$ to $n = 50$ elements [Colour figure can be viewed at wileyonlinelibrary.com]

The finding that $n = 32$ yields a sufficient result for $\omega = 0°$ aligns with recommendations for other local fatigue assessment methods found in literature, including the effective notch stress method.[44,47,48] For the opening angle $\omega = 135°$, only 24 quadratic elements per 360° are required because of the circular arc being modelled with four elements; this was also found to be sufficient for the effective notch stress method.[49,50] Thus, on the basis of

the aim of less than 1% deviation for effective stress from the converged stress, $n = 24$ and $n = 32$ actually lead to the same number of elements representing the notch root. A deviation of 1% is considered small compared with the general scatter found in fatigue assessment. Moreover, mesh refinement equal to those in other methods, in conjunction with the benefit of incorporation of size effects, underlines the potential for stress gradient methods to be generally applied for notched structures.

In order to facilitate the application readiness of often-applied versions of TCD, that is, PM and LM, the previous findings of mesh refinement for effective stress calculation are subsequently applied for comparison of both methods. For this purpose, the previously determined mesh refinements, $n = 24$ and $n = 32$, are applied for the two analysed opening angles.

6 | COMPARISON OF GRADIENT METHODS

Following the investigation on required mesh refinement, this section describes the comparison of gradient methods to discuss the assumption of PM and LM yielding the same results for a ratio of $a = \rho^*/4$. For this purpose, the previously defined parameter combinations of Table 1 are investigated in conjunction with the findings of the parameter study. Figure 8A shows the first principal stress evaluation of PM and LM, where $r = 0.05$ mm and $\omega = 0°$. This figure includes two x-axes scaled with the above-mentioned ratio between a and ρ^*, according to the assumption of Taylor and Hoey.[41] The resulting stresses indicate a clear deviation. The deviation decreases for larger distances to the root of the notch, especially in the case of sharp notches, which are related to the high stress gradient in depth direction. The parameter combination of $r = 0.05$ mm and $\omega = 135°$ (Figure 8B) shows the same general trend of the stress gradient. On the other hand, it is interesting to note that $r = 0.5$ mm and $\omega = 0°$ (Figure 8D) yield almost equal stress values for small evaluation lengths of $\rho^* = 0.05$ mm and $a = 0.0125$ mm. This is followed by a brief increase then subsequent decrease in deviation. This will be revisited later for further explanation.

The results of the von Mises stresses in Figure 9 also support the hypothesis of inequality for the two methods.

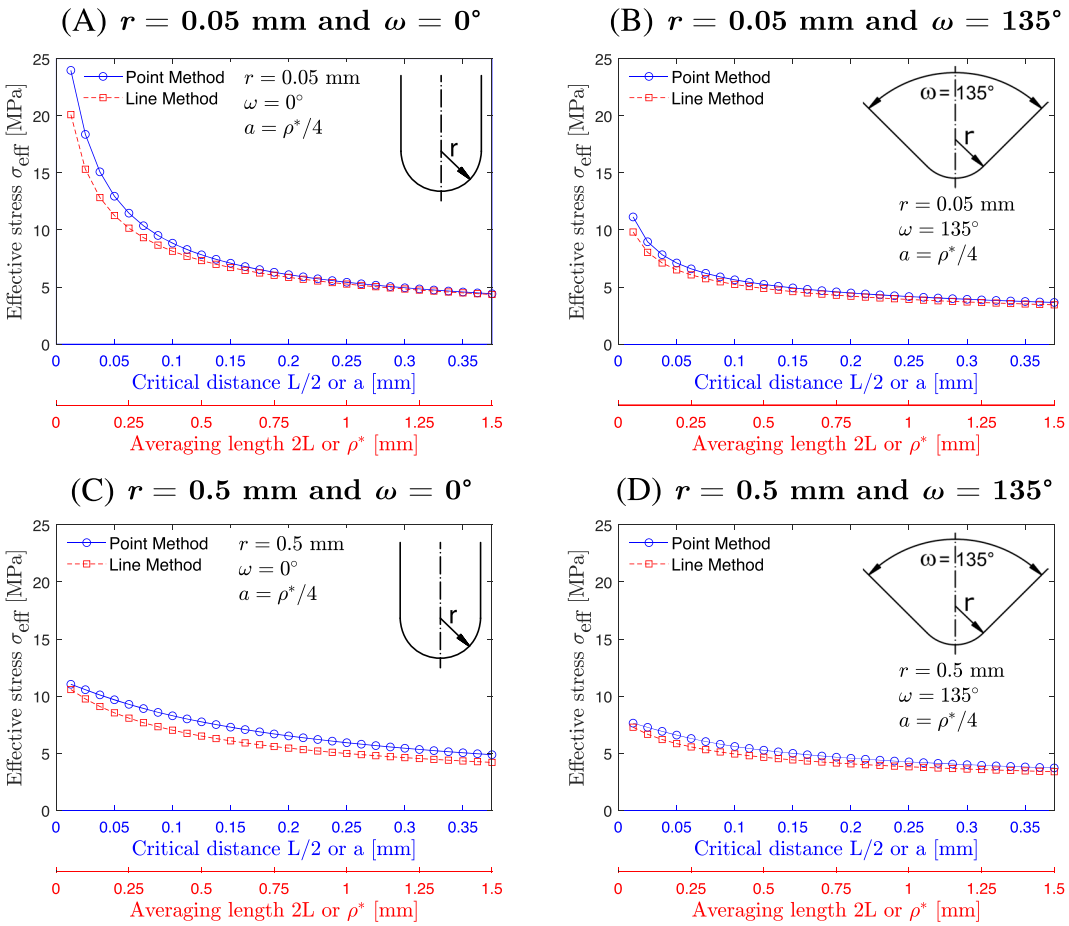

FIGURE 8 First principal stress graphs of point method (PM) and line method (LM) with a ratio of $a = \rho^*/4$ for the four different notch configurations [Colour figure can be viewed at wileyonlinelibrary.com]

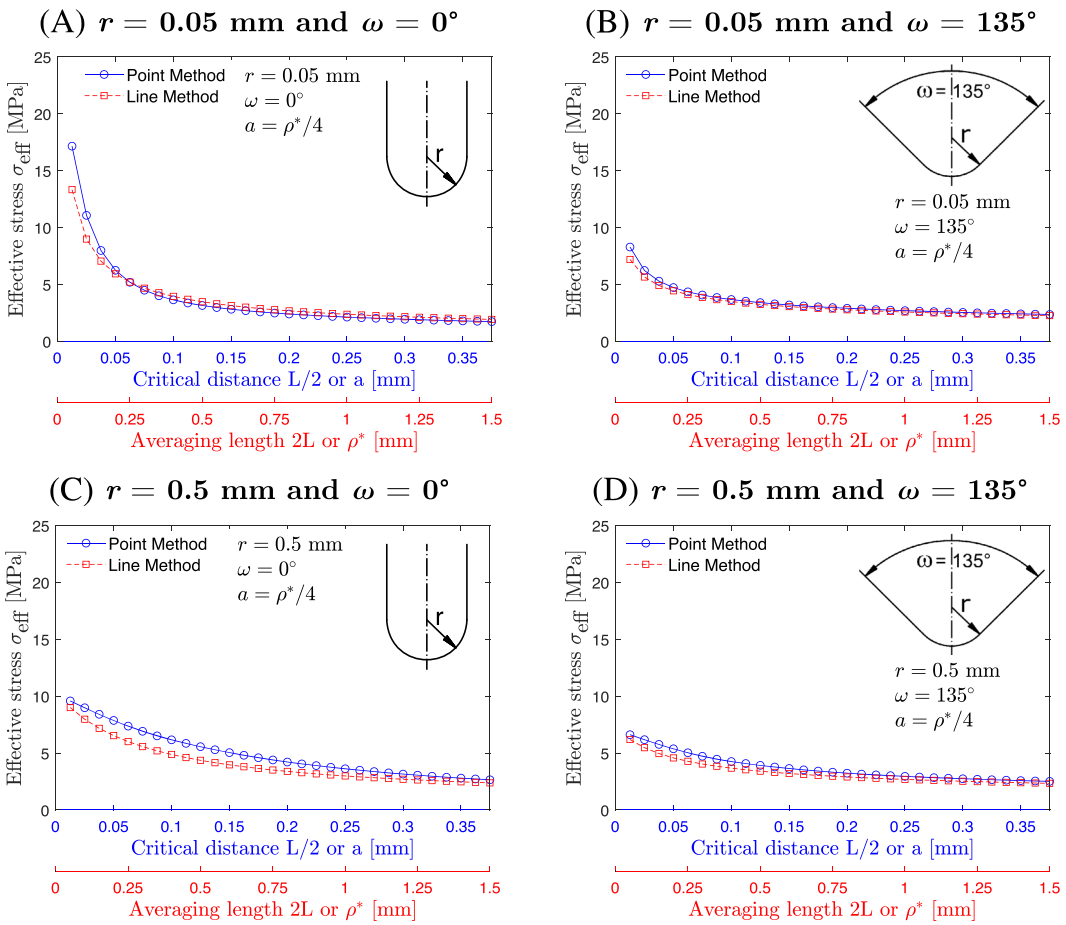

FIGURE 9 Von Mises stress graphs of point method (PM) and line method (LM) with a ratio of $a = \rho^*/4$ for the four different notch configurations [Colour figure can be viewed at wileyonlinelibrary.com]

Moreover, the diagrams present a similar trend for the same radii and opening angles compared with the first principal stress graphs in Figure 8.

In order to further illustrate the deviation between the two methods, Figure 10 presents the percent deviation (defined as deviation $= 1 - \sigma_{\text{eff,PM}}/\sigma_{\text{eff,LM}}$) between both methods for first principal stress (Figure 10A) and von Mises stress (Figure 10B). In none of these evaluated cases does the deviation approach zero for long material characteristic lengths ρ^* or a. For first

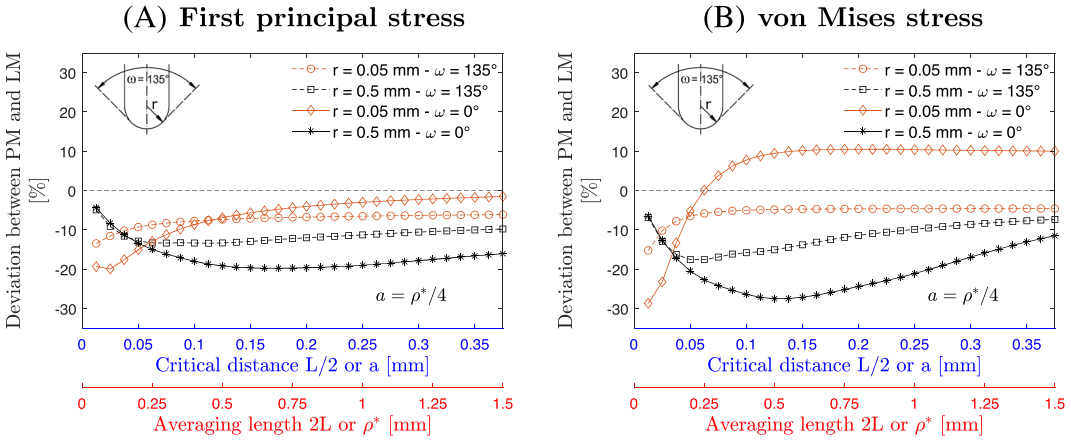

FIGURE 10 Deviation between point method (PM) and line method (LM) with a ratio of $a = \rho^*/4$ for first principal stress (A) and von Mises stress (B) [Colour figure can be viewed at wileyonlinelibrary.com]

principal stress, the parameter combination with minimal deviation (1.5%) is $r = 0.05$ mm and $\omega = 0°$, at $\rho^* = 1.5$ mm and $a = 0.375$. At the same time, this parameter combination leads to the biggest deviation of 19.9% at $\rho^* = 0.1$ mm and $a = 0.025$ mm. It is also worth noting that the curves for the same radii show similar trends, which can be explained by the radius of the notch being the main parameter governing notch sharpness. Interestingly, the graphs show a declining deviation for increasing material characteristic length for $r = 0.05$ mm. This is due to the small radius of the notch creating steep stress gradient. The graphs for $r = 0.5$ mm, however, show a slight initial deviation that first increases before it subsequently decreases again.

Within the range of the investigated parameters, $a = \rho^*/4$ never leads to the same stress values for the PM and LM, thus supporting the hypothesis that there is no constant ratio $a = \rho^*/4$ between both methods. The different trends for sharp and blunt notches can be explained by the varying degree of notch acuity, and thereby initial steepness of the stress gradient. As can be seen from Figures 8 and 9, the stress gradients are far steeper for $r = 0.05$ mm compared with $r = 0.5$ mm. This, in conjunction with the idea behind the LM of averaging the stress over a certain length, causes the different general trends in Figure 10A,B.

For sharp notches and von Mises stress results, the highest deviation is found to be close to 30% when $\rho^* = 0.05$ mm. The highest deviation for blunt notches (approximately 27.5%) is found at $\rho^* = 0.5$ mm and $a = 0.125$ when $r = 0.5$ mm and $\omega = 0°$. On the other hand, $r = 0.05$ mm and $\omega = 0°$ results in almost no deviation (0.0015%) when $\rho^* = 0.25$ mm and $a = 0.0625$. Thus, both the largest and smallest deviations are found for von Mises stress criterion. Depending on radius r and opening angle ω, as well as distance a and ρ^*, even higher deviations are theoretically possible. Nearly all cases show deviations between PM and LM; the sole exception to this occurs when $\rho^* = 0.25$ mm and $a = 0.0625$ mm for von Mises stress criterion with $r = 0.05$ mm and $\omega = 0°$. On the basis of the assumed ratio of $a = \rho^*/4$, PM usually results in higher stresses calculations than LM.

7 | DISCUSSION

The calculated difference is highest for von Mises stress criterion and blunt notches, with up to 27.5%; this is interesting to note because literature data based on fatigue tests do not always show such a clear trend.[17,20,42] Notch acuity levels, material, and specimen geometry may be responsible for this difference. Moreover, as this study has shown, a certain degree of mesh refinement is required to allow accurate calculation of effective stresses based on stress gradient methods. Consequently, different numerical modelling strategies might have also affected the outcome of other studies—for example, Susmel and Taylor[42] and Louks and Susmel[20] reported error intervals of about 20%.

For a slope of S-N curve of $k = 4$—as proposed by Baumgartner et al.[9]—a 20% difference in effective stress assessed by the TCD results in more than a 100% difference in the predicted lifetime of welded joints. This, however, leads to question which ratio ($q = a/\rho^*$) is required to obtain the same stress values for both methods when considering the investigated distances from the notch and whether there is a general relation between the two (i.e., equal stress results of the PM and LM). These questions are investigated in Figure 11, where the required ratio q to obtain the same stress values for PM and LM ($\sigma_{\text{eff,PM}} = \sigma_{\text{eff,LM}}$) is presented over the averaging length ρ^* of the LM.

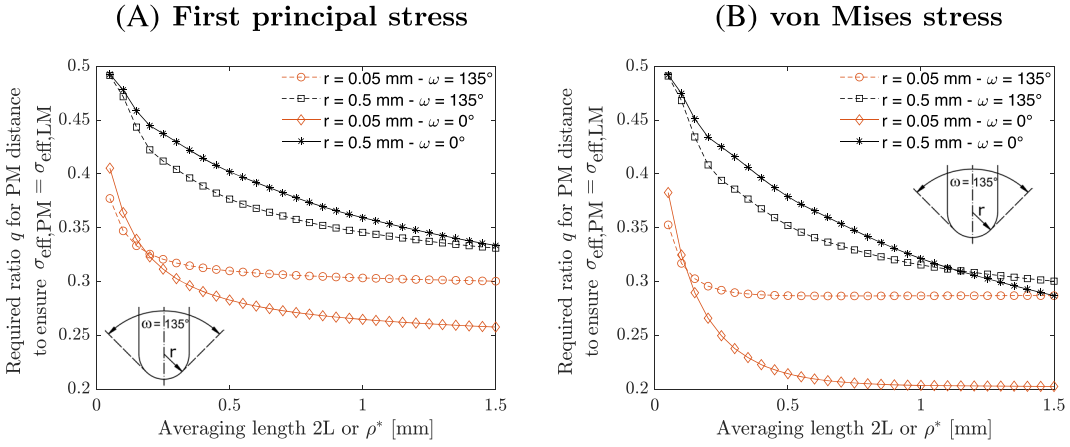

FIGURE 11 Required ratio q for point method (PM) distance a to ensure the same stress values for both methods: First principal stress (A) and von Mises stress (B) [Colour figure can be viewed at wileyonlinelibrary.com]

The ratio q never reaches a value of 1/4 within the investigated range for first principal stress, which confirms the findings from the previous investigations. For $r = 0.05$ mm and $\omega = 0$ at $\rho^* = 1.5$ mm, however, a ratio of $q = 0.257$ is found; this is relatively close to the assumed ratio. It is also worth noting that, in all cases, the biggest deviation occurs closest to the root of the notch. Thereafter, a steady decline can be observed. Furthermore, for both opening angles when $r = 0.05$ mm, an almost constant ratio q between PM and LM is observed for long material characteristic lengths L ($q = 0.257$ for $\omega = 0°$ and $q = 0.3$ for $\omega = 135°$). In contrast, the trends for $r = 0.5$ mm show a continuously decreasing ratio q at $\rho^* = 1.5$ mm. Moreover, the ratio q for short and long L ($\rho^* = 0.05$ mm and $\rho^* = 1.5$ mm) is almost equal for both opening angles. Between these two points, the deviation between the curves initially increases before approaching each other again. On the other hand, the trends for $r = 0.05$ mm are initially similar but subsequently diverge. In general, the difference between solutions for the two investigated opening angles is higher for the smaller notch radius of $r = 0.05$ mm. The observations on first principal stress described so far can also be seen in the trends of von Mises stress curves in Figure 11B. As opposed to first principal stress, the ratio yielding the same results for both methods seem to converge when $r = 0.05$ mm for lengths longer than $\rho^* = 0.5$ mm for $\omega = 135°$ and $\rho^* = 1.5$ mm for $\omega = 0°$.

First principal stress results for plane stress material behaviour (e.g., thin plates) are identical to plane strain material behaviour; however, a smaller difference between PM and LM for von Mises stress results is observed throughout the analysed range of material characteristic lengths, as can be seen in Figure 12.

On the basis of Figure 11 and Figure 12, no general conclusion can be drawn regarding the required ratio q for the parameter a in order to achieve the same effective stress value by PM and LM. A converged value can only be found in a few cases within the investigated range. Furthermore, the ratios q differ for the same radii as well as opening angles. Therefore, the only connection observed is the similarity of curves for the same radii. From the observed trend in Figure 11A,B, it seems questionable whether the results of both methods can be directly compared on the basis of a simple conversion (as assumed by Taylor and Hoey[41]); however, it is important to mention that there are reported results where their hypothesis was confirmed based on fatigue test data on seam welded joints.[9]

In order to analyse the applicability of TCD methods for fatigue assessment, the determined requirements for stress gradient based fatigue assessment of notched structures according to TCD need to be applied to fatigue test data. For this purpose, fatigue test data obtained for butt-welded joints with artificial notches obtained by Fischer et al.[45] and fatigue test data at low temperatures[51] are currently assessed and will be published in the near future.

Finally, it is important to understand that the changing ratio q over the distance of up to 1.5 mm has a significant effect on all kinds of applications. Materials with high static strength, such as metals, usually possess rather short microstructural support lengths (i.e., below $\rho^* = 0.5$ mm[37]), and the magnitude of microstructural support lengths for adhesive bonds can reach values in the range of millimetres.[8]

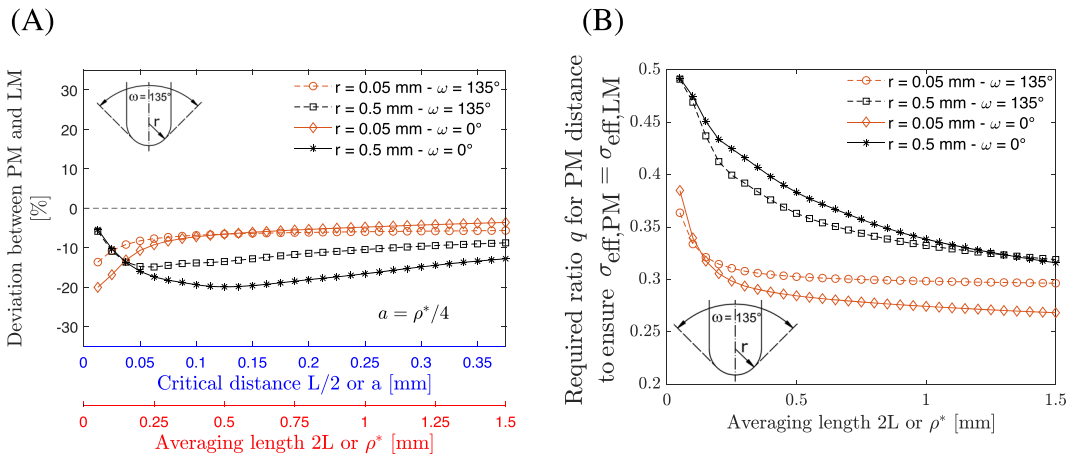

FIGURE 12 (A) Deviation between line method (LM) and point method (PM) for plane stress material behaviour with the von Mises strength hypothesis and (B) required ratio q for PM distance a to ensure the same stress values [Colour figure can be viewed at wileyonlinelibrary.com]

8 | CONCLUSIONS

In this study, the requirements for fatigue assessment by means of stress gradient methods according to the TCD were investigated with regard to mesh requirements for numerical simulation and differences in prediction accuracy between the two most commonly applied versions of the TCD—PM and LM. The following conclusions can be drawn from the investigations:

- On the basis of a parameter study, it was found that 32 elements over 360° are sufficient to calculate effective stresses that deviate less than 1% from the converged stress value for sharp notches. For blunt notches, 24 eight-node elements over 360° are sufficient with an aspect ratio of one. The difference from the converged stress is considered small compared with the differences in calculated effective stress between both analysed methods.
- In order to calculate effective stresses from steep stress gradients, PCHIP curve fitting is recommended to preserve the shape of the stress data curve.
- Furthermore, a difference in effective stress of up to 30%, and hence a significant difference in fatigue life (e.g., 185% for a slope of S-N curve of $k = 4$), can be observed for PM and LM results with the assumed ratio of $a = \rho^*/4$. For plane strain material behaviour, the difference between the methods is higher for von Mises stress than for first principal stress.
- A smaller difference between the methods is observed for plane stress material behaviour.
- Within the investigated range of material characteristic lengths, up to 1.5 mm, the required ratio between a and ρ^* is constantly changing and only converges in a few cases. Thus, it does not seem possible to harmonize both methods; different S-N curves are thus required for the two methods.

ACKNOWLEDGEMENTS

The work was performed within the research project ESM-50 'Fatigue of welded structures at sub-zero temperatures', funded by the German Research Association of the Working Group of the Iron- and Metal-processing Industry e.V. as part of the Donors' Association for the Promotion of Sciences and Humanities in Germany under project number AVIF-No. A301.

AUTHOR CONTRIBUTIONS

Conceptualization and methodology: S. E. and W. F. *Model development*: A.-S. M., A. M. M and M. B. *Investigation*: M. B. and A. M. M. *Writing*: M. B. and A. M. M. All authors have read and agreed to the published version of the manuscript.

NOMENCLATURE

a	critical distance parameter
d	notch depth
e_g, e_1, e	global element size, element size at outer radius and element size at inner radius
FAT	fatigue strength class
g	specimen height at smallest cross-section
h	specimen height
k	slope exponent of a stress-life (S-N) curve
K_t	elastic stress concentration factor
K_f	fatigue notch factor
L	material characteristic length
LM	line method
n	number of elements
N	number of cycles to failure
N_R	reference number of cycles to failure
PCHIP	piecewise cubic hermite interpolating polynomial
PM	point method
q	ratio between effective stress according to point and line method
r	notch radius
TCD	theory of critical distance
ΔK_{th}	fatigue crack growth threshold
$\Delta\sigma_R$	reference fatigue strength
$\Delta\sigma_{eff}$	effective stress range
$\Delta\sigma_0$	fatigue limit
θ, s	polar coordinates (angle and distance)
ρ^*	microstructural support length
σ_{eff}, $\sigma_{eff,max}$, $\sigma_{eff,norm}$	effective stress, maximum effective stress and normalized effective stress
$\sigma_{eff,LM}$, $\sigma_{eff,PM}$	effective stress according to line and point method
φ	supplementary angle to notch opening angle
ω	notch opening angle

ORCID

Moritz Braun https://orcid.org/0000-0001-9266-1698
Sören Ehlers https://orcid.org/0000-0001-5698-9354

REFERENCES

1. Neuber H. *Kerbspannungslehre Grundlagen für genaue Festigkeitsberechnung mit Berücksichtigung von Konstruktionsform und Werkstoff*. 2nd ed. Berlin, Heidelberg: Springer; 1958.
2. Taylor D. *The Theory of Critical Distances: A New Perspective in Fracture Mechanics*. Amsterdam: Elsevier; 2007.

3. Härkegård G, Halleraker G. Assessment of methods for prediction of notch and size effects at the fatigue limit based on test data by Böhm and Magin. *Int J Fatigue*. 2010;32(10):1701-1709.
4. Radaj D. *Design and Analysis of Fatigue Resistant Welded Structures*. Cambridge: Woodhead Publishing; 1990.
5. Zhang GB. Method of effective stress for fatigue: part I—a general theory. *Int J Fatigue*. 2012;37:17-23.
6. Berto F, Lazzarin P, Radaj D. Fictitious notch rounding concept applied to sharp V-notches: evaluation of the microstructural support factor for different failure hypotheses. Part I: basic stress equations. *Eng Fract Mech*. 2008;75(10):3060-3072.
7. Radaj D, Vormwald M. *Advanced Methods of Fatigue Assessment*. Berlin Heidelberg: Springer-Verlag; 2013.
8. Schmidt H, Baumgartner J, Melz T. Fatigue assessment of joints using the local stress field. *MATERIALWISS WERKST*. 2015;46(2):145-155.
9. Baumgartner J, Schmidt H, Ince E, Melz T, Dilger K. Fatigue assessment of welded joints using stress averaging and critical distance approaches. *Weld World*. 2015;59(5):731-742.
10. Baumgartner J, Schnabel K, Huberth F. Fatigue assessment of EMPT-welded joints using the reference radius concept. *Procedia Eng*. 2018;213:418-425.
11. Baumgartner J, Yıldırım HC, Barsoum Z. Fatigue strength assessment of TIG-dressed welded steel joints by local approaches. *Int J Fatigue*. 2019;126:72-78.
12. Marulo G, Baumgartner J, Frendo F. Fatigue strength assessment of laser welded thin-walled joints made of mild and high strength steel. *Int J Fatigue*. 2017;96:142-151.
13. Braun M, Grimm J-H, Milaković A-S, Hoffmeister, H., Canaletti, A., Ehlers, S. and Fricke, W. Bewertung der Schwingfestigkeit ausgeschliffener Schweißnähte aus hochfesten Stählen und Vergleich mit gekerbten Grundmaterialproben. 19. Tagung Schweißen in der maritimen Technik und im Ingenieurbau; 2019.
14. Karakaş Ö, Zhang G, Sonsino CM. Critical distance approach for the fatigue strength assessment of magnesium welded joints in contrast to Neuber's effective stress method. *Int J Fatigue*. 2018;112:21-35.
15. Liinalampi S, Remes H, Lehto P, Lillemae I, Romanoff J, Porter D. Fatigue strength analysis of laser-hybrid welds in thin plate considering weld geometry in microscale. *Int J Fatigue*. 2016;87:143-152.
16. Al Zamzami I, Susmel L. On the use of hot-spot stresses, effective notch stresses and the point method to estimate lifetime of inclined welds subjected to uniaxial fatigue loading. *Int J Fatigue*. 2018;117:432-449.
17. Santus C, Taylor D, Benedetti M. Experimental determination and sensitivity analysis of the fatigue critical distance obtained with rounded V-notched specimens. *Int J Fatigue*. 2018;113:113-125.
18. Spaggiari A, Castagnetti D, Dragoni E, Bulleri S. Fatigue life prediction of notched components: a comparison between the theory of critical distance and the classical stress-gradient approach. *Procedia Eng*. 2011;10:2755-2767.
19. Benedetti M, Fontanari V, Santus C, Bandini M. Notch fatigue behaviour of shot peened high-strength aluminium alloys: experiments and predictions using a critical distance method. *Int J Fatigue*. 2010;32(10):1600-1611.
20. Louks R, Susmel L. The linear-elastic theory of critical distances to estimate high-cycle fatigue strength of notched metallic materials at elevated temperatures. *Fatigue Fract Eng Mater Struct*. 2015;38(6):629-640.
21. Beber VC, Schneider B, Brede M. Efficient critical distance approach to predict the fatigue lifetime of structural adhesive joints. *Eng Fract Mech*. 2019;214:365-377.
22. Zhang GB, Sonsino CM, Sundermeier R. Method of effective stress for fatigue: part II—applications to V-notches and seam welds. *Int J Fatigue*. 2012;37:24-40.
23. Justo J, Castro J, Cicero S. Notch effect and fracture load predictions of rock beams at different temperatures using the theory of critical distances. *Int J Rock Mech min Sci*. 2020;125:1-15.
24. Li WC, Susmel L, Askes H, Liao FF, Zhou TH. Assessing the integrity of steel structural components with stress raisers using the theory of critical distances. *Eng Fail Anal*.. 2016;70:73-89.
25. Faruq NZ, Susmel L. Proportional/nonproportional constant/-variable amplitude multiaxial notch fatigue: cyclic plasticity, non-zero mean stresses, and critical distance/plane. *Fatigue Fract Eng Mater Struct*. 2019;42(9):1849-1873.
26. Luo P, Yao WX, Susmel L, Li P. Prediction methods of fatigue critical point for notched components under multiaxial fatigue loading. *Fatigue Fract Eng Mater Struct*. 2019;42(12):2782-2793.
27. Muñiz-Calvente M, Álvarez-Vázquez A, Cicero S, et al. Study of the influence of notch radii and temperature on the probability of failure: a methodology to perform a combined assessment. *Fatigue Fract Eng Mater Struct*. 2019;42(12):2663-2673.
28. Mei J, Xing S, Vasu A, Chung J, Desai R, Dong P. The fatigue limit prediction of notched components—a critical review and modified stress gradient based approach. *Int J Fatigue*. 2020;135:1-15.
29. Pereira JCR, de Jesus AMP, Xavier J, Correia JAFO, Susmel L, Fernandes AA. Low and ultra-low-cycle fatigue behavior of X52 piping steel based on theory of critical distances. *Int J Fatigue*. 2020;134:1-9.
30. Hobbacher AF. Comparison of fatigue verification procedures at a thick-walled welded component. *Weld World*. 2017;61(4):801-818.
31. Hobbacher AF. *Recommendations for Fatigue Design of Welded Joints and Components*. 2nd ed. Switzerland: Springer International Publishing; 2016.
32. DNVGL-RP-0005:2014–06: Fatigue design of offshore steel structures. 2014.
33. BS EN 1993–1–9:2005 – Eurocode 3: Design of Steel Structures—Part 1–9: Fatigue. 2008.
34. Radaj D, Sonsino CM, Fricke W. *Fatigue assessment of welded joints by local approaches*. 2nd ed. Cambridge: Woodhead publishing; 2006.
35. Peterson RE. Notch sensitivity. In: Sines G, Lwaisman J, eds. *Metal Fatigue*. New York: McGraw-Hill; 1959:293-306.
36. Radaj D, Lazzarin P, Berto F. Generalised Neuber concept of fictitious notch rounding. *Int J Fatigue*. 2013;51:105-115.
37. Neuber H. Über die Berücksichtigung der Spannungskonzentration bei Festigkeitsberechnungen. *Konstruktion*. 1968;20(7):245-251.
38. Kuguel R. A relation between theoretical stress concentration factor and fatigue notch factor deduced from the concept of

highly stressed volume. In: *ASTM Proceeding 1961*. Vol.61 ASTM International; 1961:732-748.
39. Wormsen A, Sjödin B, Härkegård G, Fjeldstad A. Non-local stress approach for fatigue assessment based on weakest-link theory and statistics of extremes. *Fatigue Fract Eng Mater Struct*. 2007;30(12):1214-1227.
40. Lazzarin P, Tovo R. A unified approach to the evaluation of linear elastic stress fields in the neighborhood of cracks and notches. *Int J Fract*. 1996;78(1):3-19.
41. Taylor D, Hoey D. High cycle fatigue of welded joints: the TCD experience. *Int J Fatigue*. 2009;31(1):20-27.
42. Susmel L, Taylor D. A novel formulation of the theory of critical distances to estimate lifetime of notched components in the medium-cycle fatigue regime. *Fatigue Fract Eng Mater Struct*. 2007;30(7):567-581.
43. Eichlseder W. Fatigue analysis by local stress concept based on finite element results. *Comput Struct*. 2002;80(27–30):2109-2113.
44. Baumgartner J, Bruder T. An efficient meshing approach for the calculation of notch stresses. *Welding in the World*. 2012;57(1):137-145.
45. Fischer C, Fricke W, Rizzo CM. Fatigue tests of notched specimens made from butt joints at steel. *Fatigue Fract Eng Mater Struct*. 2016;39(12):1526-1541.
46. Baumgartner J. *Schwingfestigkeit von Schweißverbindungen unter Berücksichtigung von Schweißeigenspannungen und Größeneinflüssen*. Stuttgart: Fraunhofer Verlag; 2014.
47. Leitner M, Pauer P, Kainzinger P, Eichlseder W. Numerical effects on notch fatigue strength assessment of non-welded and welded components. *Comput Struct*. 2017;191:51-61.
48. Eibl M, Sonsino CM, Kaufmann H, Zhang G. Fatigue assessment of laser welded thin sheet aluminium. *Int J Fatigue*. 2003;25(8):719-731.
49. Fricke W. *IIW recommendations for the fatigue assessment of welded structures by notch stress analysis: IIW-2006-09*. Cambridge: Woodhead Publishing; 2012.
50. Fricke W. Round-Robin study on stress analysis for the effective notch stress approach. *Welding in the World*. 2013;51(3–4):68-79.
51. Braun M, Scheffer R, Fricke W, Ehlers S. Fatigue strength of fillet-welded joints at subzero temperatures. *Fatigue Fract Eng Mater Struct*. 2020;43(2):403-416.

How to cite this article: Braun M, Müller AM, Milaković A-S, Fricke W, Ehlers S. Requirements for stress gradient-based fatigue assessment of notched structures according to theory of critical distance. *Fatigue Fract Eng Mater Struct*. 2020;43:1541–1554. https://doi.org/10.1111/ffe.13232